Differential cross sections for the electron-impact excitation of hydrogenlike carbon

C.P. Bhalla and S.R. Grabbe
J. R. Macdonald Laboratory, Department of Physics, Kansas State University, Manhattan, Kansas 66506-2604

A.K. Bhatia
Laboratory for Astronomy and Solar Physics, NASA, Goddard Space Flight Center, Greenbelt, Maryland 20771
(Received 5 April 1995)

We report on a study of total and differential excitation cross sections for the electron-impact excitation of hydrogenlike carbon for the transitions $1s\,^2S \rightarrow 2s\,^2S$ and $2p\,^2P$. These calculations have been performed for electron-impact energies ranging from 28.2 to 29.5 Ry using the close-coupling R-matrix method. This energy region has been chosen because in addition to the direct excitation of $2s$ and $2p$, there is a sizable contribution to the excitation cross section from the doubly excited two-electron states ($3l3l'$), which decay predominantly to $n = 2$ via autoionization. Differential cross sections both for the direct nonresonant channel and in the vicinity of several autoionizing resonant states are presented. The differential cross sections in the vicinity of the autoionizing resonant states are shown to be very rich in structure. We discuss the relevance of these calculations to a recent experiment that measured the electron emission spectra for the collision of $C^{5+}+H_2$.

PACS number(s): 34.80.Kw, 34.50.Fa, 32.80.Hd

I. INTRODUCTION

An understanding of inelastic electron-ion collisions is of fundamental importance for diagnosing laboratory and astrophysical plasmas. Due to very low ion target densities, experimental studies of electron-impact excitation of ions are extremely difficult. Despite these difficulties, several experimental [1–4] and theoretical studies [5–12] have been published that report total excitation cross sections.

However, measurements of inelastic differential scattering cross sections (DCS's) have only been reported for a very limited number of electron-ion collision systems. Chutjian and co-workers [13–15] have reported inelastic DCS's for a range of angles extending from 4° to 17° for $Zn^+(4s \rightarrow 4p)$, $Cd^+(5s \rightarrow 5p)$, and $Mg^+(3s \rightarrow 3p)$. The energy of the incident electrons in these experiments ranged from 30 to 100 eV, which is well above the excitation threshold, and they found that the inelastically scattered electrons were peaked in the direction of the incident beam. Huber *et al.* [16] have reported inelastic DCS's for the $3s \rightarrow 3p$ excitation of sodiumlike Ar^{7+} at angles ranging from 13° to 39°. This experiment was performed at 100 eV which is again well above the excitation threshold, and the measured DCS's peaked around 20°. Finally, Dunn and co-workers [1,17] have been able to deduce the "gross features" of the inelastic DCS's for $Ar^{7+}(3s \rightarrow 3p)$ and $O^{5+}(2s \rightarrow 2p)$ near the excitation threshold and have found that the inelastic DCS's tend to be very strongly peaked in the backward direction at these low energies.

As a result of the limited number of inelastic DCS measurements for electron-ion collisions, relatively few theoretical studies have been performed. Among the theoretical studies, several different models have been used in the calculation of inelastic DCS's. Close-coupling results have been reported by Griffin and co-workers [18–20] for Si^{2+}, Ar^{6+}, Ar^{7+}, Zn^+, and Li^+. Berrington and co-workers [21,22] have also reported close-coupling results for He^+ and Li^+. Among the authors using the distorted-wave approximation to calculate inelastic DCS's are Zou and Shirai [23], who have performed extensive calculations for H-like ions, Itikawa and co-workers [24–26], who have reported studies for He-like ions and H-like ions, and Pangantiwar and Srivastava [27], who have calculated inelastic DCS's for $Zn^+(4s \rightarrow 4p)$, $Cd^+(5s \rightarrow 5p)$, and $Mg^+(3s \rightarrow 3p)$, which agree very well with the experimental work of Chutjian and co-workers [13–15]. Finally, Herviuex and Guet [28] have calculated DCS's for the excitation of alkalilike ions by electron impact using the generalized Born approximation and a semiclassical approximation and were able to show that the two approximations give very similar angular distributions. To determine the differences between these various models, Griffin and Pindzola [20] have compared nonunitarized distorted-wave, unitarized distorted-wave, and close-coupling calculation and have found that the inelastic DCS's can be significantly different, although the total excitation cross sections are in good agreement. Similarly, Pindzola *et al.* [29] have compared inelastic DCS's calculated using a quantal distorted-wave approximation and a classical-trajectory Monte Carlo method and have found the classical results to be qualitatively in agreement with the quantal distorted-wave calculations, but the classical results are unable to reproduce the detailed diffraction pattern of the DCS's. It should be noted that all of the theoretical studies mentioned so far deal exclusively with the angular differential cross sections for nonresonant excitation and to our knowledge only the study of Griffin *et al.* [30] examines the angular DCS's in the vicinity of autoionizing resonance transitions. Griffin *et al.* [30] have calculated angular DCS's

for the transitions $3s^2\ ^1S \rightarrow 3s3p\ ^3P$, $3s^2\ ^1S \rightarrow 3s3p\ ^1P$, and $3s3p\ ^3P \rightarrow 3s3p\ ^1P$ in the Mg-like ions Si^{2+} and Ar^{6+}. These calculations have been carried out in the threshold energy region, which has been shown to exhibit strong resonance structures for both ions. Due to the lack of studies regarding the angular DCS's for resonant contributions to excitation, considerably more theoretical and experimental work needs to be done in this area.

It is the purpose of this paper to present total and differential inelastic scattering cross sections for the $1s \rightarrow 2s$ and $2p$ excitation of C^{5+} for impact energies between 28.2 and 29.5 Ry. We report on the effects of interference between the direct excitation and the autoionization channels on the DCS's. Contribution to the excitation cross section from the doubly excited two-electron states $(3l3l')$ that decay predominantly to $n = 2$ via autoionization is also presented. The relevance of these calculations to a recent experiment [33] is also discussed.

In Sec. II we discuss our calculational method followed by results and a discussion of the total and differential cross sections for $e+C^{5+}$ in Sec. III A. Section III B contains doubly differential cross sections for $C^{5+} + H_2$, and we present a summary of our results in Sec. IV.

II. CALCULATION METHODS

The electron-impact excitation cross section was calculated in the close-coupling approximation using the R-matrix method of Berrington *et al.* [34,35]. The total $(N+1)$-electron wave function for the collision system can be described within the LS-coupling scheme as

$$\Psi_k(x_1,\ldots,x_{N+1}) = \mathcal{A}\sum_{i,j} c_{ijk}\chi_i(x_1,\ldots,x_n;\hat{r}_{N+1},\sigma_{N+1})r_{N+1}^{-1}u_{ij}(r_{N+1}) + \sum_j d_{jk}\Psi_j(x_1,\ldots,x_{N+1}) , \quad (1)$$

where χ_i are the target orbitals coupled to the spin-angle function of the free electron, u_{ij} are the continuum basis orbitals, $\mathcal{A}$ is the antisymmetrization operator, and Ψ_j are the bound-state $(N+1)$-electron wave functions. The lowest 15 hydrogenlike orbitals, up to $n = 5$, have been used to represent the target in the R-matrix internal region. For the present calculation, the R-matrix boundary radius is taken at 13 a.u. and 40 continuum orbitals have been included in the expansion of the total wave function. All $(N+1)$-electron symmetries with even and odd parities up to total angular momentum $L= 12$ were used. For impact energies up to 29.5 Ry, the calculation of partial waves to $L = 12$ is sufficient to ensure the convergence of the cross sections.

We have written a program to calculate DCS's that is similar to an earlier program written by Salvini [36] and have followed his theoretical formalism. We denote the initial target state as N_i with orbital angular momentum L_{N_i} and spin momentum S_{N_i}. The final target state is labeled N_f with orbital angular momentum L_{N_f} and spin momentum S_{N_f}. The initial and final orbital angular momenta of the scattered electron are designated by l_i and l_f, the momentum transfer is $\vec{j}_t = \vec{l}_f - \vec{l}_i = \vec{L}_{N_i} - \vec{L}_{N_f}$, and k_{N_i} is the wave vector of the incident electron. The total orbital and spin angular momenta and parity of the electron-target system are given by L, S, and Π, respectively.

Angular DCS's can be calculated by taking the axis of quantization along the electron-beam direction and the scattering angle θ is defined with respect to this axis. The DCS at an angle θ for inelastic scattering from an initial state N_i to a final state N_f within the LS-coupling scheme can be written as

$$\frac{d\sigma}{d\Omega}(N_i \rightarrow N_f|\theta) = \sum_\lambda A_\lambda(N_i \rightarrow N_f)P_\lambda(\cos\theta) , \quad (2)$$

where $P_\lambda(\cos\theta)$ are Legendre polynomials of order λ and the A_λ are given by

$$A_\lambda(N_i \rightarrow N_f) = \frac{1}{8k_{N_i}^2[L_{N_i}][S_{N_i}]} \sum_{\substack{l_i,l_f,\bar{l}_i,\bar{l}_f \\ S,j_t}} i^{(l_i-l_f+\bar{l}_f-\bar{l}_i)}\ e^{i(\sigma_{l_i}+\sigma_{l_f}-\sigma_{\bar{l}_i}-\sigma_{\bar{l}_f})} \times (-1)^{j_t+\lambda}\,[j_t]\,C_{000}^{l_i\bar{l}_i\lambda}\,C_{000}^{l_f\bar{l}_f\lambda}W(l_il_f\bar{l}_i\bar{l}_f;j_t\lambda)M_{\bar{l}_i\bar{l}_f}^{Sj_t*}(N_i \rightarrow N_f)\,M_{l_il_f}^{Sj_t}(N_i \rightarrow N_f) . \quad (3)$$

$C_{m_i,m_f,m}^{l_i,l_f,l}$ and $W(abcd;ef)$ are the Clebsch-Gordan and Racah coefficients, respectively. Notice that when the Fano-Racah convention is used, the factor $i^{(l_i-l_f+\bar{l}_f-\bar{l}_i)}$ is set equal to unity in the expression for A_λ. The Coulomb phase shifts are defined as $\sigma_l = \arg\Gamma(l+1-i\alpha)$, where $\alpha = q/k_{N_i}$, with q as the asymptotic charge of the target, and k_{N_i} is given by

$$k_{N_i}^2 = k^2 + 2(E_{N_i} - E_{N_f}). \quad (4)$$

k^2 is the energy of the incident electron and E_{N_i} and E_{N_f} are the energies of the N_ith and N_fth target state.

The M matrices are defined as

$$M_{l_il_f}^{Sj_t}(N_i \rightarrow N_f) = ([l_i][l_f][S])^{1/2}\sum_{L\pi}(-1)^L\,[L] \times W(l_iL_{N_i}l_fL_{N_f};Lj_t) \times T_{l_il_f}^{LS\pi}(N_i \rightarrow N_f) . \quad (5)$$

The transition matrix elements $T_{l_il_f}^{LS\pi}(N_i \rightarrow N_f)$ for $e + C^{5+}$ were calculated using the R-matrix codes developed by Berrington *et al.* [35].

III. RESULTS AND DISCUSSION

A. Total and differential cross sections for $e + C^{5+}(1s)$

The collision strengths for this study were calculated using the R-matrix codes developed by Berrington *et al.* [35]. Our calculations for the $1s \rightarrow 2s$ and $1s \rightarrow 2p$ transitions in the energy region of interest are in excellent agreement with those calculated by Aggarwal and Kingston [31], who also used the R-matrix approach. These results agree to within 10% with the pseudostate expansion calculations of Abu-Salbi and Callaway [32].

We have chosen to present the results from the R-matrix calculations in terms of total cross sections. The relationship between the total cross section and the collision strength is given by

$$\Omega_{ij} = \omega_i k_i^2 \sigma_{ij} (\pi a_0^2), \quad (6)$$

where ω_i is the statistical weight of the initial state and k_i^2 is the energy of the incident electron in rydbergs. In Fig. 1, the total excitation cross sections for the $1s \rightarrow 2s$ and $1s \rightarrow 2p$ transitions in units of πa_0^2 are plotted as a function of the electron-impact energy. In order to accurately represent both the position and shape of each resonance appearing between 28.2 and 29.5 Ry, we have calculated the total excitation cross section with an energy mesh of 0.0025 Ry.

The very rich resonance structure dominating the excitation cross sections between 28.2 and 29.5 Ry is associated with the process

$$e + C^{5+}(1s) \rightarrow C^{4+}(3l3l') \rightarrow C^{5+}(2l) + e\,. \quad (7)$$

We have identified the ten resonances appearing in Fig. 1 by the following procedure. We calculated the energies, autoionization rates, and radiative rates for all states belonging to the $3l3l'$ complex making use of the Hartree-Fock model with the inclusion of electron-configuration mixing. In all cases, the Auger branching ratio to the ground state is much smaller than to the $n = 2$ states. If one were to ignore the interference effects, the cross section to $n = 2$ would be proportional to the product of the Auger rate to the ground state times the branching ratio to $2l$. By examining this product, we can identify the $3l3l'$ states that will be significant in the total $2s$ and $2p$ excitation cross sections. The observed doubly excited $3l3l'$ states are labeled in Table I and the energy positions of these doubly excited states are compared to theoretical calculations by van der Hart and Hansen [37]. The truncated diagonalization method with a second-order energy correction in a B-spline basis has been used by van der Hart and Hansen [37] to calculate the energies of the $3l3l'$ singlet levels of C^{4+}. They have compared their energies with calculations by Martín *et al.* [38], Abu-Salbi and Callaway [32], and Ho [39,40] and have found their energies to be in excellent agreement with these earlier calculations.

First we present DCS's for the $1s \rightarrow 2s$ and $2p$ transitions at two energies where only the direct excitation

TABLE I. Identification and energy in rydbergs for the $3l3l'$ doubly excited states compared with calculated values of van der Hart and Hansen [37] for singlet states.

Peak no.	State	Present	Hart and Hansen
1	$3s^2\ ^1S$	28.573	28.575
2	$3s3p\ ^3P$	28.593	
3	$3p^2\ ^1D$	28.650	28.655
4	$3s3p\ ^1P$	28.710	28.722
5	$3p3d\ ^3F$	28.733	
6	$3s3d\ ^3D$	28.773	28.779[a]
7	$3d^2\ ^1D$	28.850	28.862
8	$3p3d\ ^1F$	28.985	29.002
9	$3s3d\ ^1D$	29.100	29.126
10	$3p3d\ ^1P$	29.173	29.196

[a]Ho and Bhatia, Ref. [43].

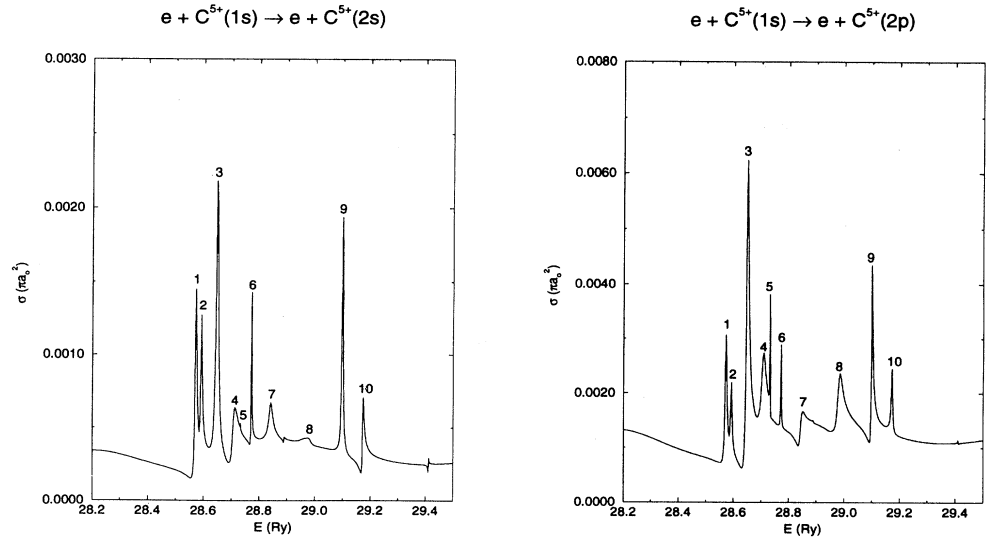

FIG. 1. Electron-impact total cross sections in πa_0^2 versus electron-impact energy in rydbergs for $1s \rightarrow 2s$ and $1s \rightarrow 2p$ excitations.

channel is open. Figure 2 contains the DCS's versus scattering angle for an impact energy of 27.2 Ry, which lies well below the energy region where resonances associated with the $3l3l'$ manifold are found. Note that the DCS's are very strongly peaked in the backward direction for both the $1s \rightarrow 2s$ *and* $2p$ transitions. In Fig. 3, the DCS's versus scattering angle are plotted at 29.49 Ry, which is higher than the $3p3d\ ^1P$ resonance but below the $3l4l'$ series of resonances. For the $1s \rightarrow 2s$ transition, the DCS's are strongly peaked in the forward direction, but the DCS's for $1s \rightarrow 2p$ exhibit only a slight forward peaking.

The DCS's versus scattering angle are presented for the following resonances: $3s^2\ ^1S$, $3p^2\ ^1D$, $3p3d\ ^1F$, and $3s3d\ ^1D$ in Figs. 4–7. These resonances correspond to peaks 1, 3, 8, and 9 in Fig. 1.

The angular distribution of the (Auger) electron resulting from the deexcitation of the doubly excited $3l3l'$ states to the $2l$ states can be used in elucidating the resonance structure appearing in the DCS's, calculated with the inclusion of the interference between the direct nonresonant and resonant amplitudes. In general, Auger electrons resulting from the depopulation of a doubly excited resonant state will have a nonisotropic angular distribution that depends on the magnetic substrate population of the doubly excited state. If the doubly excited state is labeled by LSM_LM_S, the final state after Auger decay is labeled by $L''S''M_L''M_S''$, and the outgoing electron is labeled by lsm_lm_s, then the angular distribution of the Auger electron is given in atomic units by [41]

$$W(\theta) = 2\pi[J''][L][S] \sum_{M,M'',m_s} P(SLJM) \left| \sum_l (+i)^l e^{i\delta_l} e^{-im_l} Y_{l,m_l}(\theta,\phi) A(SL \rightarrow S''L'', sl) \right.$$
$$\left. \times \sum_{M_S,M_L} \sum_{M_S'',M_L''} \begin{pmatrix} L'' & S'' & J'' \\ M_L'' & M_S'' & -M'' \end{pmatrix} \begin{pmatrix} S'' & s & S \\ M_S'' & m_s & -M_S \end{pmatrix} \begin{pmatrix} L'' & l & L \\ M_L'' & m_l & -M_L \end{pmatrix} \begin{pmatrix} L & S & J \\ M_L & M_S & -M \end{pmatrix} \right|^2, \quad (8)$$

where $\begin{pmatrix} j_1 & j_2 & j_3 \\ m_1 & m_2 & -m_3 \end{pmatrix}$ is the $3j$ symbol of Wigner, $[j] = 2j+1$, $A(SL \rightarrow S''L'', sl)$ is the transition amplitude, and $P(SLJM)$ is the magnetic substrate population of the doubly excited state. Since the orbital magnetic quantum number of the outgoing electron is equal to zero when the axis of quantization is taken along the beam direction, one finds that when only one partial wave contributes in Eq. (8), the angular distribution of the outgoing electron at the resonant energy is given by

$$W(\theta) \sim |Y_{l,0}(\theta,\phi)|^2 \quad (9)$$

when the interference between the direct nonresonant and resonant amplitudes is ignored.

For an electron-impact energy corresponding to the $3s^2\ ^1S$ resonance, the DCS's to both $2s$ and $2p$ are shown by a solid line in Fig. 4. In this and the following three figures, the solid curve will correspond to the DCS at the resonance energy, the dotted curve will correspond to the DCS at an energy 0.01 Ry lower than the resonance energy, and the dashed curve corresponds to the DCS at an energy 0.01 Ry higher than the resonance energy. Based on the above considerations [Eq. (8)], the angular differential cross section for the inelastically scattered electron

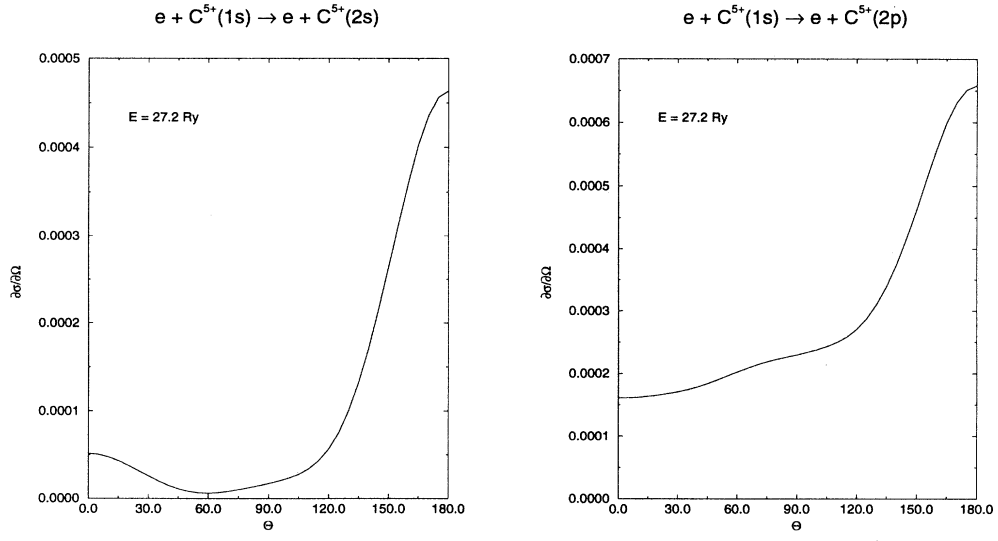

FIG. 2. Differential cross sections in a.u./sr versus scattering angle in degrees at 27.2 Ry, which lies below the observed resonance structure associated with the $3l3l'$ doubly excited states, for $1s \rightarrow 2s$ and $1s \rightarrow 2p$ excitations.

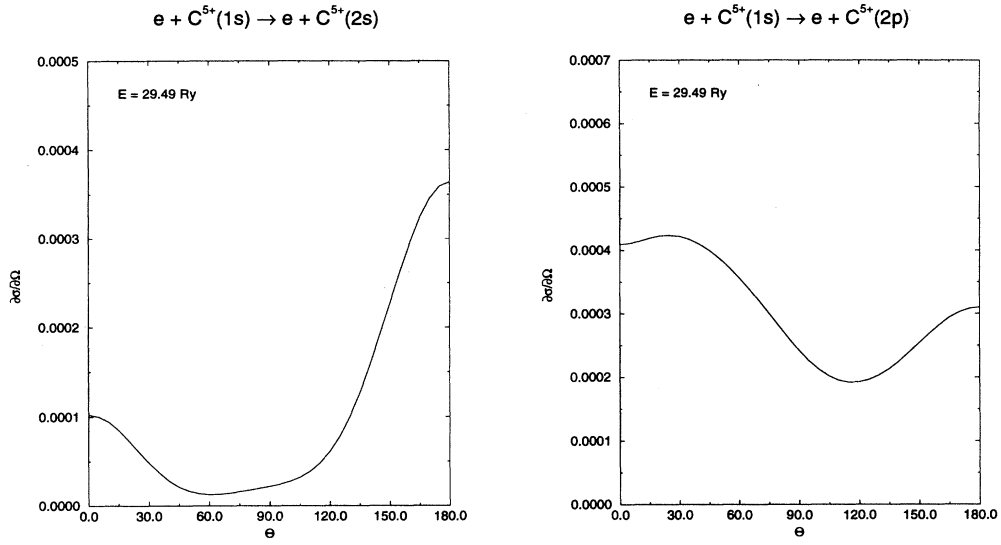

FIG. 3. Differential cross sections in a.u./sr versus scattering angle in degrees at 29.4 Ry, which lies above the observed resonance structure associated with the $3l3l'$ doubly excited states, for $1s \rightarrow 2s$ and $1s \rightarrow 2p$ excitations.

at the $3s^2\ ^1S$ resonance is expected to be isotropic. The structure appearing in Fig. 4(a) is due to the interference between the resonant and the direct nonresonant channels. For $3s^2\ ^1S \rightarrow 2p\ ^2P + e$, the angular distribution of the inelastically scattered electron according to Eq. (8) is given by $|Y_{1,0}|^2$, which is zero and symmetric about 90°. The asymmetry of the DCS in Fig. 4(b) at large and small scattering angles is due to interference. The sensitivity of the DCS in the vicinity of a resonance is also shown in Fig. 4.

The calculated DCS for the $3p^2\ ^1D$ resonance is plotted in Fig. 5. For excitation to $2s$, the angular distribution from Eq. (8) has the form $|Y_{2,0}|^2$, which has minima at $\sim 54.74°$ and $\sim 125.26°$. The asymmetry observed at large and small scattering angles in Fig. 5(a) is again due to interference between the direct nonresonant and resonant channels.

For the $3p3d\ ^1F$ resonance, the DCS to $2s$ versus scattering angle is shown in Fig. 6(a). The angular distribution is $|Y_{3,0}|^2$ according to Eq. (8). The dramatic deviation of the DCS from this shape is indicative of the strong interference between the direct nonresonant channel and the resonant channel.

For the $3s3d\ ^1D$ resonance, the angular DCS's to both $2s$ and $2p$ are presented in Fig. 7. The angular distribution for $3s3d\ ^1D \rightarrow 2s\ ^2S + e$ is expected to be $|Y_{2,0}|^2$, ignoring the interference between the resonant and nonresonant channels.

For the last three resonances discussed above, there are always two partial waves that are relevant in Eq. (8) for the $1s \rightarrow 2p$ transition. The angular distribution for such cases depends on the matrix elements appropriate to the deexcitation of these states to $2p$ and is not discussed here.

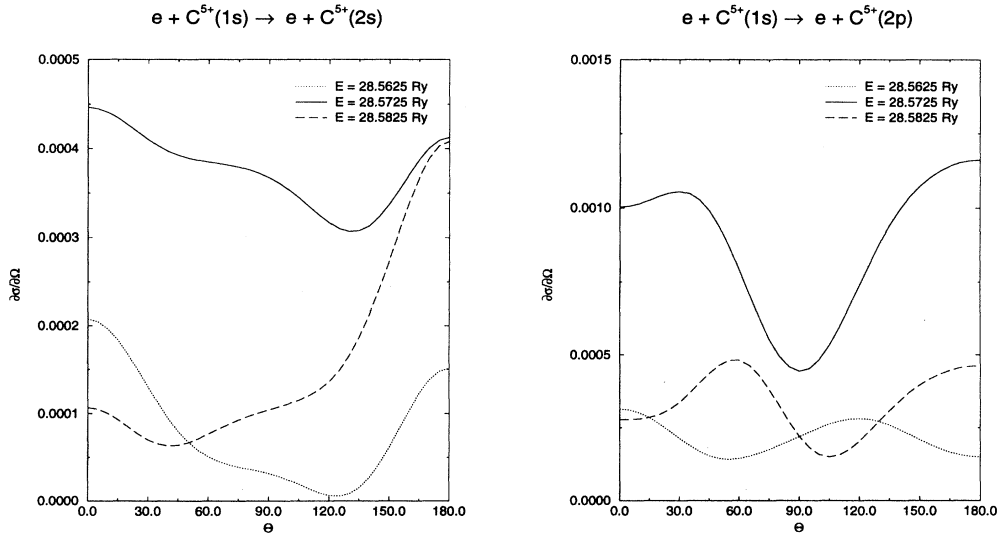

FIG. 4. Differential cross sections in a.u./sr versus scattering angle in degrees in the vicinity of the $3s^2\ ^1S$ resonance for $1s \rightarrow 2s$ and $1s \rightarrow 2p$ excitations. Solid curve, calculations at resonance; dotted curve, calculations at 0.01 Ry below resonance; dashed curve, calculations at 0.01 Ry above resonance.

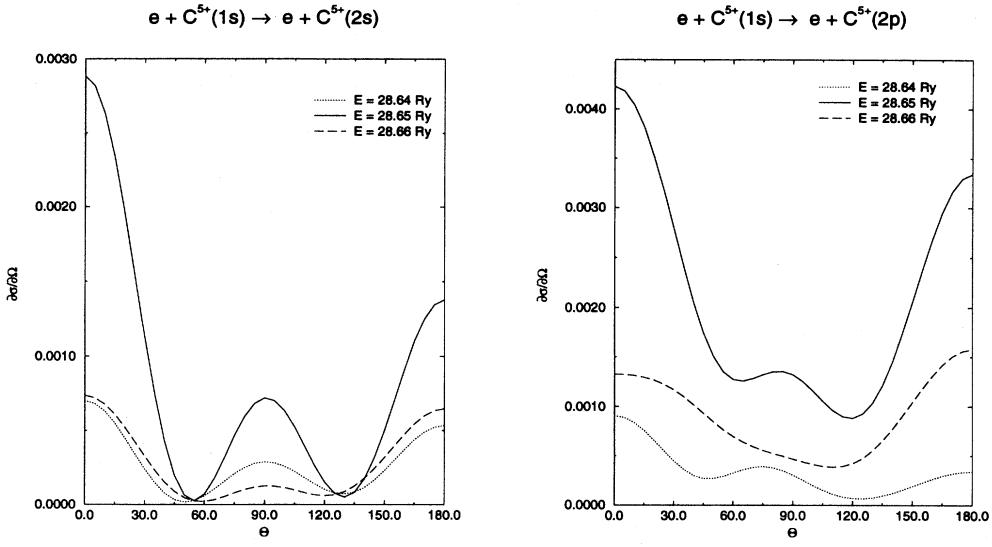

FIG. 5. Same as Fig. 4, but for $3p^2\ ^1D$.

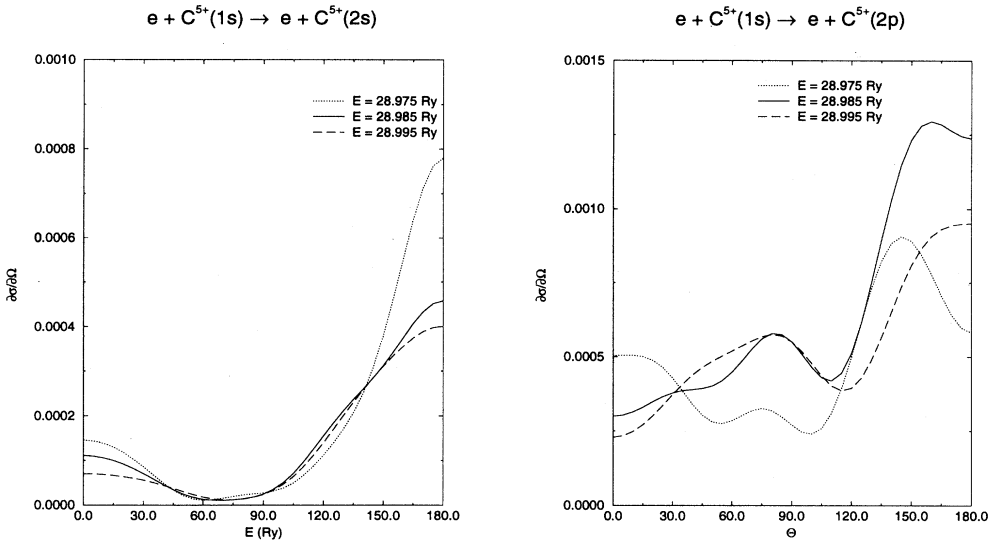

FIG. 6. Same as Fig. 4, but for $3p3d\ ^1F$.

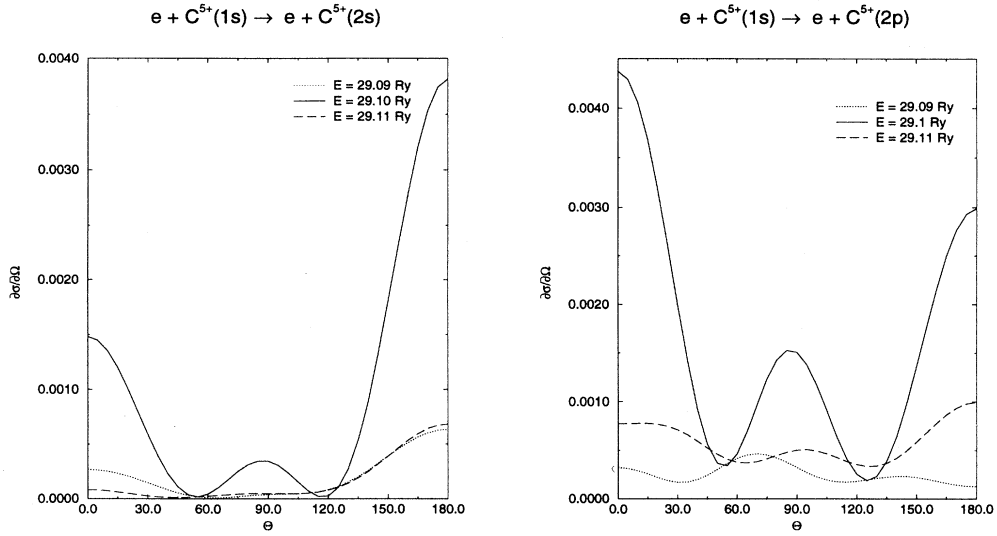

FIG. 7. Same as Fig. 4, but for $3s3d\ ^1D$.

To add further insight into the nature of the interference between the direct nonresonant channel and the resonant channel, the DCS's at fixed angles are presented as a function of the electron-impact energy between 28.2 and 29.5 Ry. The DCS for the $1s \rightarrow 2s$ transition is presented at 5° and 50° in Fig. 8 and at 90° and 178° in Fig. 9. Notice the dramatic decrease in magnitude for many of the resonances in Figs. 8 and 9. This decrease at 50° can partly be understood by noting that the angular distribution without interference for $3p^2\ ^1D$, $3s3d\ ^3D$, $3d^2\ ^1D$, and $3s3d\ ^1D \rightarrow 2s + e$ is expected to be of the form $|Y_{2,0}|^2$, which vanishes at $\sim 54.74°$. Simi-

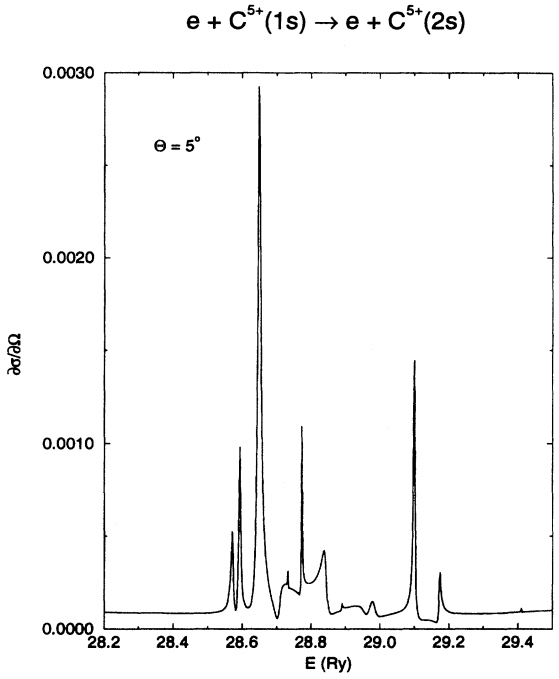

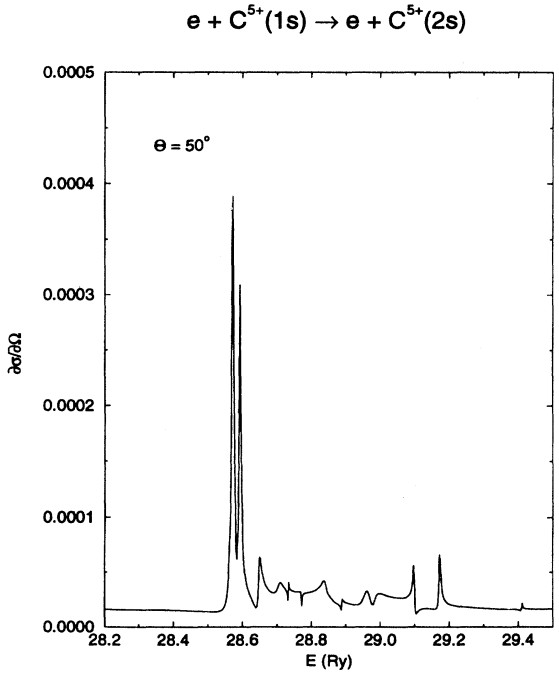

FIG. 8. Differential cross sections in a.u./sr versus electron-impact energy in rydbergs for $1s \rightarrow 2s$ at $\theta = 5°$ and $\theta = 50°$.

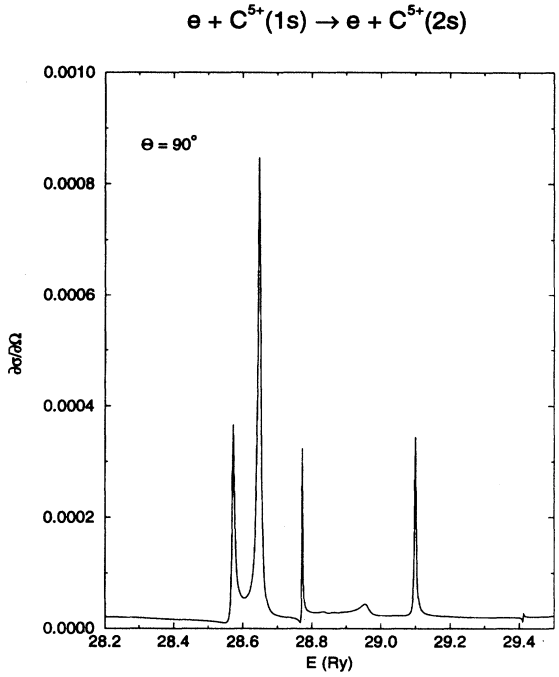

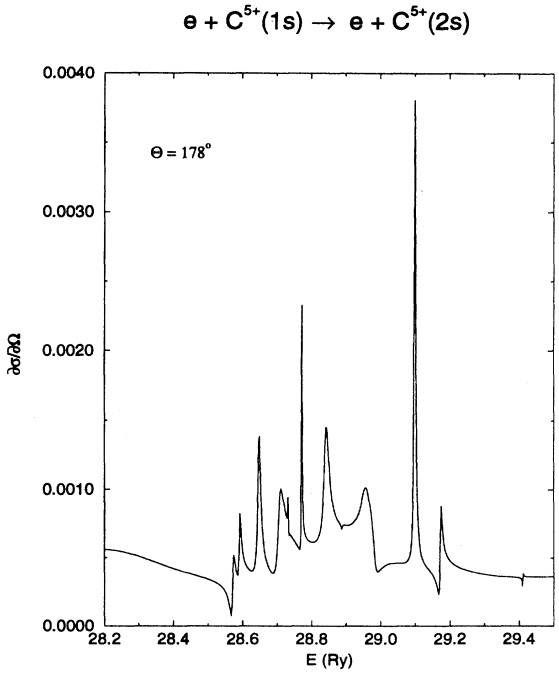

FIG. 9. Differential cross sections in a.u./sr versus electron-impact energy in rydbergs for $1s \rightarrow 2s$ at $\theta = 90°$ and $\theta = 178°$.

larly, this decrease in the DCS for the $3s3p\ ^3P$, $3s3p\ ^1P$, and $3p3d\ ^1P$ resonances at 90° corresponds qualitatively to an angular distribution $|Y_{1,0}|^2$. Similar considerations are valid for the $3p3d\ ^3F$ and $3p3d\ ^1F$ resonances. The strong backward peaking of the DCS for $1s \rightarrow 2s$ is apparent in Fig. 9.

The energy differential inelastic cross sections for $1s \rightarrow 2p$ at 5°, 50°, 90°, and 178° are plotted in Figs. 10 and 11. Strong interference effects can be seen between the direct nonresonant channel and the resonant channel. Note the pronounced Fano-type profile appearing at $\sim$ 25.55 Ry at 5° and 178°, which is associated with the interference

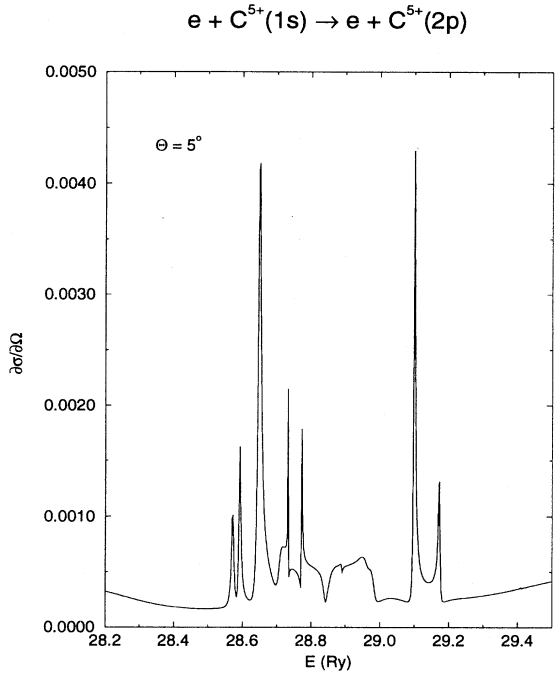

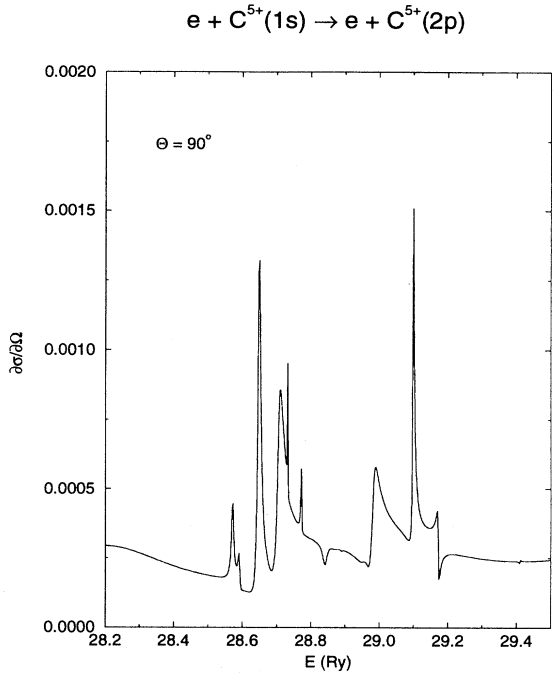

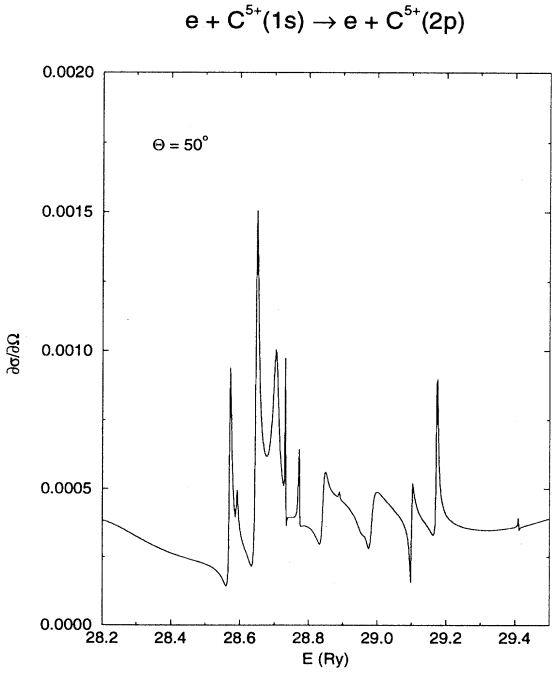

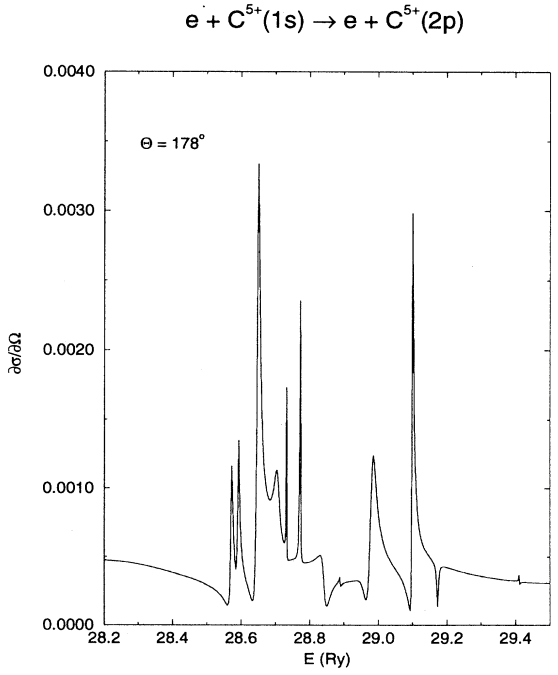

FIG. 10. Differential cross sections in a.u./sr versus electron-impact energy in rydbergs for $1s \rightarrow 2p$ at $\theta = 5°$ and $\theta = 50°$.

FIG. 11. Differential cross sections in a.u./sr versus electron-impact energy in rydbergs for $1s \rightarrow 2p$ at $\theta = 90°$ and $\theta = 178°$.

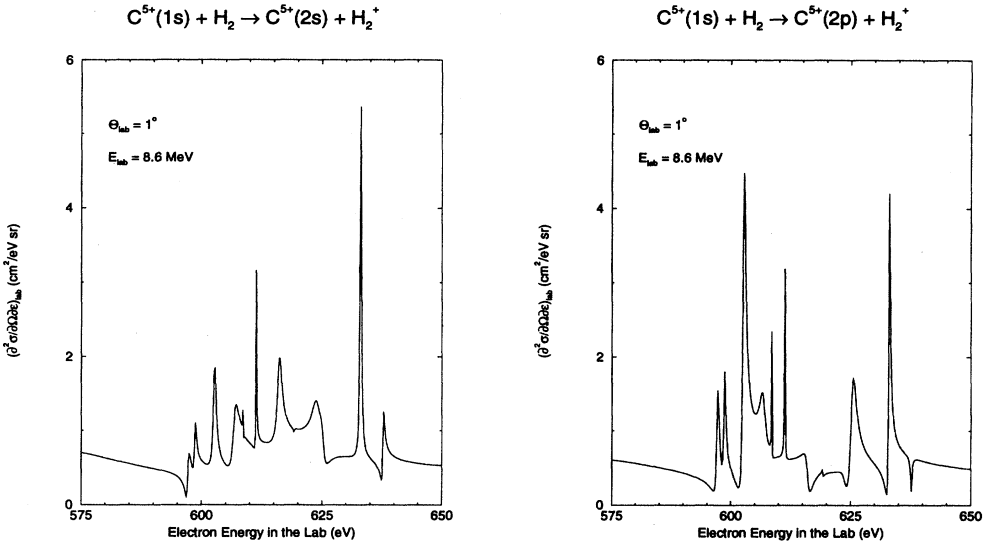

FIG. 12. Doubly differential cross sections in 10^{-21} cm^2/eV sr versus laboratory electron energy at $\theta_{\rm lab} = 1°$ for 8.6-MeV $C^{5+}(1s) + H_2 \rightarrow C^{5+}(2s) + H_2{}^+ + e$ and $C^{5+}(1s) + H_2 \rightarrow C^{5+}(2p) + H_2{}^+ + e$.

between the direct excitation channel and the $3s^2\ {}^1S$ resonances.

The strong resonance structure appearing between 28.2 and 29.5 Ry makes this collision system an excellent candidate for future electron-ion experiments. The calculated DCS's that we have presented can provide important information regarding the planning of experiments and designed to measure the differential inelastic scattering cross sections for electron-C^{5+} collisions.

B. Doubly differential cross sections for $C^{5+} + H_2$

One of the motivating factors behind this study was to calculate doubly differential electron production cross sections (DDCS's), which qualitatively reproduce the rich resonance structure observed in a recent experiment by Hvelplund *et al.* [33]. In this experiment, the electron spectra were measured at laboratory scattering angles ranging from 1° to 5° for the collision of 8.6-MeV $C^{5+} + H_2$ within the energy range of the Auger electrons corresponding to the $3l3l'$ doubly excited states of C^{4+}.

In order to calculate the DDCS, we have utilized the impulse approximation [42], which is expected to be valid when the projectile (C^{5+}) velocity is much larger than the typical electron velocity of the target atom. When this condition is satisfied, the bound electrons of the target (H_2) can be treated as quasi-free-electrons having a characteristic momentum distribution given by the Compton profile $J(Q)$. The DDCS for the ion-atom collision can then be related to the DCS for the electron-ion collision in the *projectile frame* as

$$\frac{\partial^2\sigma(\theta,\epsilon)}{\partial\Omega\partial\epsilon} = \left(\frac{\partial\sigma(\theta)}{\partial\Omega}\right)\left(\frac{J(Q)}{Q+V_p}\right), \qquad (10)$$

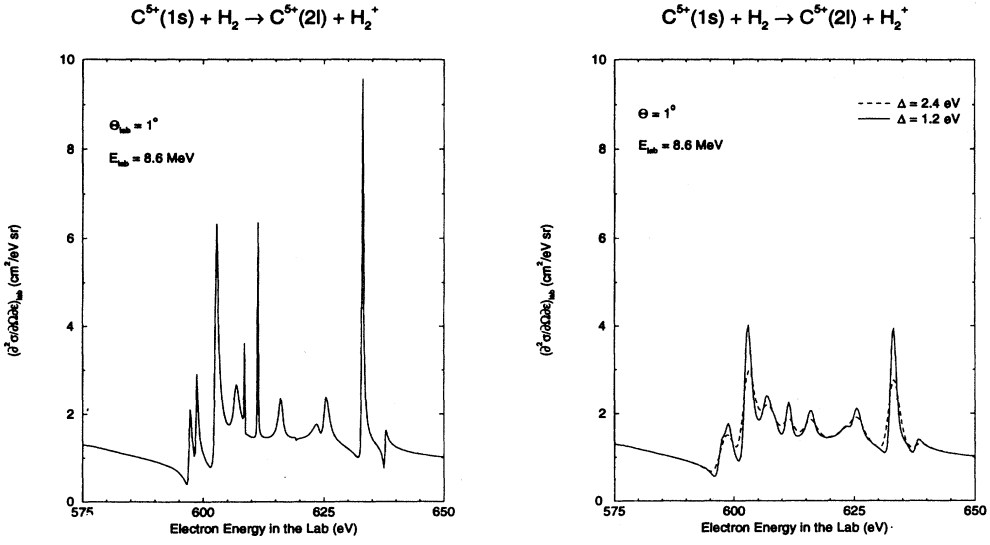

FIG. 13. Doubly differential cross sections in (10^{-21} cm^2/eV sr versus laboratory electron energy at $\theta_{\rm lab} = 1°$ for 8.6-MeV $C^{5+}(1s) + H_2 \rightarrow C^{5+}(2l) + H_2{}^+ + e$ with "infinite" resolution and $C^{5+}(1s) + H_2 \rightarrow C^{5+}(2\ell) + H_2{}^+ + e$ convoluted with a 2.4-eV FWHM Gaussian (dotted curve) and a 1.2-eV FWHM Gaussian (solid curve).

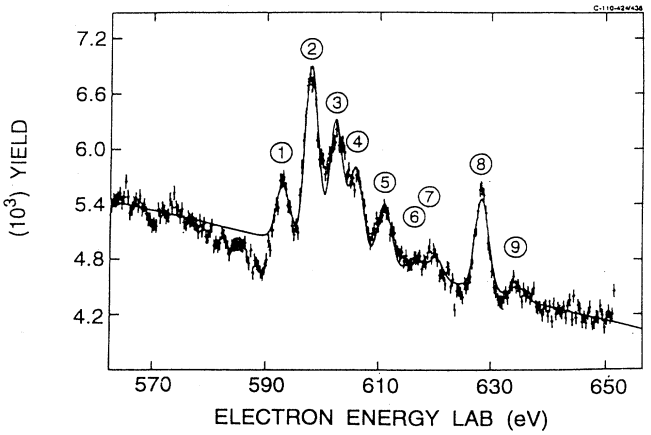

FIG. 14. Experimental electron yield versus laboratory electron energy at $\theta_{\rm lab} = 1°$ for 8.6-MeV C^{5+} collisions with molecular hydrogen as observed by Hvelplund *et al.* [33].

where V_p is the velocity of the projectile and $Q = \sqrt{2}\left(\sqrt{\epsilon + E_b} - V_p\right)$. Here ϵ is the energy of the incident electron and E_b is the binding energy of the electron. DDCS in the laboratory frame can be easily obtained from Eq. (10) by standard transformations.

In Fig. 12, we have plotted the DDCS's for the $1s \rightarrow 2s$ and $2p$ transitions for $C^{5+} + H_2$ at 8.6 MeV and $\theta_{\rm lab} = 1°$, which corresponds to a scattering angle of 178° in the projectile frame. Since the DDCS's to $2s$ and $2p$ cannot be experimentally resolved, we have plotted the DDCS for $1s \rightarrow 2l$ in Fig. 13 with "infinite" resolution and convoluted with a 1.2-eV and a 2.4-eV full width at half maximum (FWHM) Gaussian. The latter of these two resolutions is consistent with the experimentally observed resolution of 0.4% reported by Hvelplund *et al.* [33].

By comparing the DDCS of Fig. 13 with the experimental electron spectra in Fig. 4(a) of Hvelplund *et al.* [33], reproduced in Fig. 14, one sees that our calculated DDCS's do qualitatively reproduce both the positions and shapes of the experimentally observed resonance structure. A direct comparison between the calculated DDCS and the experimental electron spectrum is not possible because the electrons observed in this spectrum are due not only to the $1s \rightarrow 2l$ channel but also to a number of additional processes that give rise to electrons in this energy region. It is hoped that this study will motivate future ion-atom experiments so that a more detailed comparison can be made with theory.

IV. SUMMARY AND CONCLUSION

We have presented the results of extensive calculations on the total and differential excitation cross sections for the electron-impact excitation of hydrogenlike carbon for the transitions $1s\ ^2S \rightarrow 2s\ ^2S$ and $2p\ ^2P$. These calculations have been performed for electron-impact energies ranging from 28.2 to 29.5 Ry with an energy mesh of 0.0025 Ry using the close-coupling R-matrix method. This energy region has been chosen because in addition to the direct excitation of $2s$ and $2p$, there is a sizable contribution to the excitation cross section from the doubly excited two-electron states ($3l3l'$), which decay predominantly to $n = 2$ via autoionization. Differential cross sections for the direct nonresonant channel at electron impact energies of 27.2 and 29.49 Ry were presented. The differential cross sections for excitation to $2s$ and $2p$ show strong peaking at backward angles for an impact energy equal to 27.2 Ry. For an impact energy of 29.49 Ry, the DCS's show a similar behavior for the excitation to $2s$ in contrast to the $2p$ excitation results in which case the DCS's are peaked slightly in the forward direction. All the resonances that belong to the $3l3l'$ complex and contribute significantly to the $2s$ and $2p$ excitations are identified and the resonance energies agree very well with the accurate calculations of van der Hart and Hansen and of other authors.

The differential cross section at the resonance energy and at ±0.01 Ry with respect to the resonance energy are presented for several resonances to show the sensitivity of the DCS. We have reported on a qualitative description of the angular distribution for several cases to provide insight on the role of the interference contributions. The DCS's at fixed angles (5°, 50°, 90°, and 178°) are also presented as a function of the electron-impact energy. The resonance contribution including the Fano-type profile are strongly dependent on the observation angle. These results, which are available from the authors, can provide useful and important information in planning DCS experiments. It is our understanding that several groups are considering such experiments using the merged-beam or crossed-beam techniques.

The impulse approximation has been used to calculate DDCS's for $C^{5+}(1s) + H_2 \rightarrow C^{5+}(2l) + H_2^+$ and these DDCS's were found to qualitatively reproduce the resonant structure observed in a recent experiment reported by Hvelplund *et al.* [33] and shown in Fig. 14. A proper background subtraction is essential in the determination of the absolute cross sections. We anticipate that future ion-atom experiments will be able to provide a more stringent test of theory.

ACKNOWLEDGMENTS

We are very grateful to Professor P.G. Burke for making available to us the latest version of the R-matrix programs. It is a pleasure for us to thank T.W. Gorczyca for many useful discussions and making it possible for us to compare our differential cross section program with a program developed earlier and independently by D.C. Griffin and M.S. Pindzola, to whom we express our sincere appreciation and thanks. The contributions and assistance of K.S. Baliyan are gratefully acknowledged. The work at Kansas State University was supported by the Division of Chemical Sciences, Office of Basic Energy Sciences, Office of Energy Research, U.S. Department of Energy.

[1] E. W. Bell, X. Q. Guo, J. L. Forand, K. Rinn, D. R. Swenson, J. S. Thompson, G. H. Dunn, M. E. Bannister, D. C. Gregory, R. A. Phaneuf, A. C. H. Smith, A. Müller, C. A. Timmer, E. K. Wåhlin, B. D. DePaola, and D. S. Belić, Phys. Rev. A **49**, 4585 (1994).
[2] S. J. Smith, A. Chutjian, J. Mitroy, S. S. Tayal, R. J. W. Henry, K. F. Man, R. J. Mawhorter, and I. D. Williams, Phys. Rev. A **48**, 292 (1993).
[3] R. A. Phaneuf, in *Proceedings of the XVIII International Conference on the Physics of Electronic and Atomic Collisions*, edited by Torklid Andersen, Bent Fastrup, Finn Folkmann, Helge Knudsen, and N. Andersen, AIP Conf. Proc. No. 295 (AIP, New York, 1993), p. 405.
[4] X. Q. Guo, E. W. Bell, J. S. Thompson, G. H. Dunn, M. E. Bannister, R. A. Phaneuf, and A. C. H. Smith, in *Proceedings of the XVI International Conference on the Physics of Highly Charged Ions*, edited by P. Richard, M. Stockli, C. L. Cocke, and C. D. Lin, AIP Conf. Proc. No. 274 (AIP, New York, 1992), p. 463.
[5] D. J. Lennon and V. M. Burke, Astron. Astrophys. Suppl. Ser. **103**, 273 (1994).
[6] K. S. Baliyan and A. K. Bhatia, J. Phys. B **27**, 4281 (1994).
[7] K. M. Aggarwal and F. P. Keenan, J. Phys. B **27**, 2343 (1994).
[8] M. C. Chidichimo, D. W. Schranz, and B. Zygelman, Phys. Rev. A **48**, 4245 (1993).
[9] A. K. Bhatia and S. O. Kastner, At. Data Nucl. Data Tables **54**, 133 (1993).
[10] P. G. Burke and K. A. Berrington, *Atomic and Molecular Processes: An R-Matrix Approach* (IOP, Bristol, 1993).
[11] H. L. Zhang and A. K. Pradhan, Phys. Rev. A **50**, 3105 (1993).
[12] M. S. Pindzola, T. W. Gorczyca, D. C. Griffin, and N. R. Badnell, in *Proceedings of the XVIII International Conference on the Physics of Electronic and Atomic Collisions* (Ref. [3]), p. 415.
[13] A. Chutjian, A. Z. Msezane, and R. J. W. Henry, Phys. Rev. Lett. **50**, 1357 (1983).
[14] A. Chutjian, Phys. Rev. A **29**, 64 (1984).
[15] I. D. Williams, A. Chutjian, and R. J. Mawhorter, J. Phys. B **19**, 2189 (1986).
[16] B. A. Huber, Ch. Ristori, P. A. Hervieux, M. Maurel, C. Guet, and H. J. Andrä, Phys. Rev. Lett. **67**, 1407 (1991).
[17] X. Q. Guo, E. W. Bell, J. S. Thompson, G. H. Dunn, M. E. Bannister, R. A. Phaneuf, and A. C. H. Smith, Phys. Rev. A **47**, R9 (1993).
[18] D. C. Griffin, M. S. Pindzola, and N. R. Badnell, in *Proceedings of the XVI International Conference on the Physics of Highly Charge Ions* (Ref. [4]), p. 463.
[19] M. S. Pindzola, N. R. Badnell, R. J. W. Henry, D. C. Griffin, and W. L. van Wyngaarden, Phys. Rev. A **44**, 5628 (1991).
[20] D. C. Griffin and M. S. Pindzola, Phys. Rev. A **42**, 248 (1990).
[21] K. A. Berrington, A. E. Kingston, and S. A. Salvini, J. Phys. B **16**, 2399 (1983).
[22] S. Nakazaki and K. A. Berrington, Phys. Rev. A **43**, 3509 (1991).
[23] Yu Zou and Toshizo Shirai, Phys. Rev. A **45**, 6902 (1992).
[24] Y. Itikawa and K. Sakimoto, Phys. Rev. A **38**, 664 (1988).
[25] K. Sakimoto and Y. Itikawa, Phys. Rev. A **40**, 3646 (1989).
[26] R. Srivastava, Y. Itikawa, and K. Sakimoto, Phys. Rev. A **43**, 4736 (1991).
[27] A. W. Pangantiwar and R. Srivastava, J. Phys. B **21**, L219 (1988).
[28] P. A. Hervieux and C. Guet, Phys. Rev. A **47**, 2031 (1993).
[29] M. S. Pindzola, D. R. Schultz, and D. C. Griffin, Phys. Rev. A **48**, 4333 (1993).
[30] D. C. Griffin, M. S. Pindzola, and N. R. Badnell, Phys. Rev. A **47**, 2871 (1993).
[31] K. M. Aggarwal and A. E. Kingston, J. Phys. B **24**, 4583 (1991).
[32] N. Abu-Salbi and J. Callaway, Phys. Rev. A **24**, 2372 (1981).
[33] P. Hvelplund, A. D. González, P. Dahl, and C. P. Bhalla, Phys. Rev. A **49**, 2535 (1994).
[34] K. A. Berrington, P. G. Burke, M. Le Dourneuf, W. D. Robb, K. T. Taylor, and Vo Ky Lan, Comput. Phys. Commun. **14**, 367 (1978).
[35] K. A. Berrington, P. G. Burke, K. Butler, M. J. Seaton, P. J. Storey, K. T. Taylor, and Yu Yan, J. Phys. B **20**, 6379 (1987).
[36] S. A. Salvini, Comput. Phys. Commun. **27**, 25 (1982).
[37] H. W. van der Hart and J. E. Hansen, J. Phys. B **26**, 641 (1993).
[38] F. Martín, I. Sánchez, and H. Bachau, Phys. Rev. A **40**, 4245 (1989).
[39] Y. K. Ho, Phys. Rev. A **23**, 2137 (1981).
[40] Y. K. Ho (private communication); M. Mack, J. H. Nijland, P. van der Straten, A. Niehaus, and R. Morgenstern, Phys. Rev. A **39**, 3846 (1989).
[41] B. Cleff and W. Mehlhorn, J. Phys. B **7**, 593 (1974).
[42] See, for example, D. Brandt, Phys. Rev. A **27**, 1314 (1983); C. P. Bhalla, Phys. Rev. Lett. **64**, 1103 (1990); C. Liao, P. Richard, S. R. Grabbe, C. P. Bhalla, T. J. M. Zouros, and S. Hagmann, Phys. Rev. A **50**, 1328 (1994), and references cited therein.
[43] Y. K. Ho and A. K. Bhatia, Phys. Rev. A **44**, 2895 (1991).